European Journal of Organic Chemistry

EurJOC
European Journal of Organic Chemistry

Chemistry Europe
European Chemical Societies Publishing

RESEARCH ARTICLE OPEN ACCESS

Synthesis of DNA Building Blocks With Aminonaphthalimides and Cyanovinylenes as Uncharged Fluorophores: Fluorescent Readout From Turn-On to Red-Shift

Jan Kunzmann | Anna-Lena Ruopp | Hans-Achim Wagenknecht

Institute of Organic Chemistry, Karlsruhe Institute of Technology (KIT), Karlsruhe, Germany

Correspondence: Hans-Achim Wagenknecht (Wagenknecht@kit.edu)

Received: 17 March 2026 | **Revised:** 1 June 2026 | **Accepted:** 9 June 2026

Keywords: aminonaphthalimides | cyanovinylenes | DNA | excimers | fluorescence | H-aggregates | UV/Vis absorption

ABSTRACT

Three phosphoramidites of aminonaphthalimides and two of cyanovinylenes were synthesized as DNA building blocks and incorporated as novel fluorescent nucleotide analogs into DNA. The chromophores were attached to oligonucleotides using propanediol as acyclic linker between the phosphodiester bridges. This linker provides high stability and flexibility in comparison to the conventional 2-deoxyfuranoside; it places the chromophore as nucleotide analog into DNA and is compatible with automated oligonucleotide chemistry. For aminonaphthalimides, two different linker lengths were compared, and the role of demethylation at the exocyclic amino group was evaluated. For cyanovinylenes, the role of the alkylamino group for fluorescence response was evaluated. The exploration of the optic-spectroscopic properties of the dyes in different DNA architectures with the possibility to form interstrand and intrastrand dimers showed that aminonaphthalimides and cyanovinylenes can be used as nucleic acid-sensitive dyes by their fluorescence turn-on and red-shift as readouts. The fluorescence turn-on was tested by probing N^6-methyl-2′-deoxyadenosine (m^6A) in DNA.

1 | Introduction

Fluorescence labeling of DNA is a prerequisite for molecular diagnostics and imaging in cells. To visualize distinct DNA or RNA sequences, hybridization-sensitive probes with alterable fluorescence properties are required [1, 2]. Such changes can manifest either as variations in fluorescence intensity (turn-on) or as altered emission maximum (red-shift) [3, 4]. When a chromophore is bound or intercalated to DNA, conformational freedom is restricted; this suppression of non-radiative decay pathways from the excited state results in enhanced fluorescence intensity. Such light-up or turn-on can be applied as readout for hybridization and thus the presence of a target sequence [5]. Fluorescence red-shifts provide a more reliable readout, since they minimize misinterpretation caused by non-targeting effects that might affect and quench fluorescence at a single wavelength. A particularly effective way to achieve such red-shifts is through excimer formation, which occurs when two adjacent fluorophores interact in the excited state, producing a characteristic red-shifted emission [6, 7]. Pyrene is the most established excimer-forming dye and has been successfully incorporated into DNA [8–12]. However, pyrene suffers from significant drawbacks, including excitation in the DNA-damaging UV region and high sensitivity towards oxygen. Perylene bisimides also form excimers in DNA with red-shifted emission, but their fluorescence is strongly quenched by guanine due to photoinduced electron transfer [13, 14]. Thiazole orange (TO) is an important alternative that avoids these problems. TO can be excited at wavelengths above 450 nm and possesses a redox potential that precludes guanine oxidation. TO has already been widely

integrated into nucleic acids probes: Seitz et al. incorporated TO in PNA, and later also into DNA, to create so-called "forced intercalation thiazole (FIT) probes," which serve as powerful hybridization-sensitive RNA probes for cell imaging [15–17]. Okamoto et al. realized the "exciton-controlled hybridization-sensitive fluorescent oligonucleotide "(ECHO) concept by placing two adjacent TO fluorophores into DNA [18, 19]. We further demonstrated that two individually incorporated TO chromophores in DNA can form TO dimers in the duplex, leading to a red-shifted emission when positioned in a face-to-face arrangement [20, 21]. These dimers exhibit blue-shifted absorption and weak or symmetry-allowed emission due to excitonic coupling in the ground state.

Among excimer-forming dyes, naphthalimides and cyanovinylenes are promising dyes for novel fluorescent DNA with readout by turn-on and red-shift. Yoon and Spring reported aminonaphthalimide sensors for Cu(II) based on excimer formation [22].

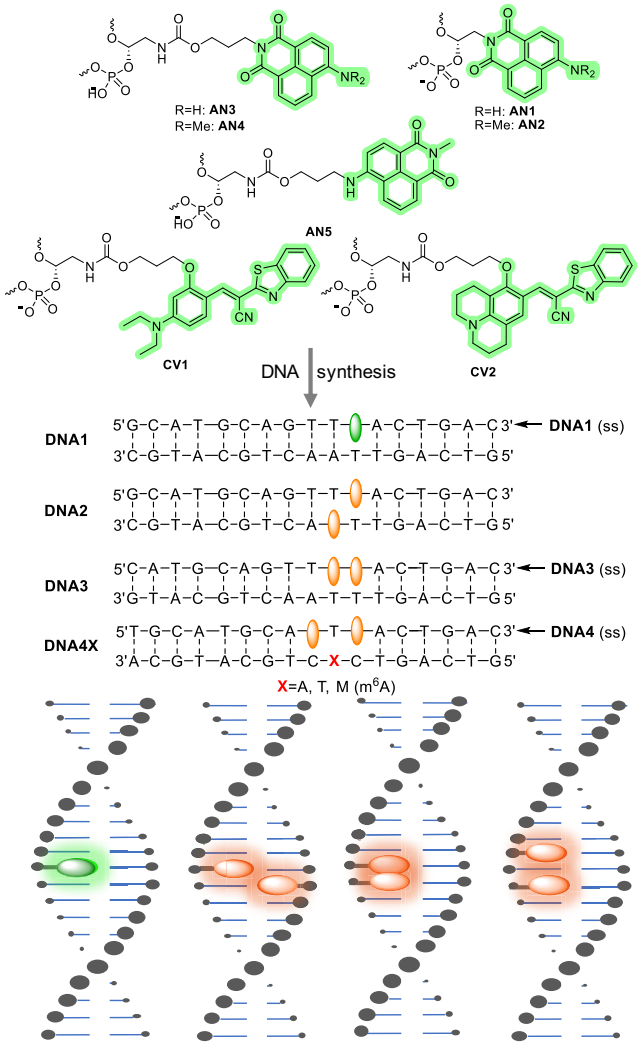

FIGURE 1 | Fluorescent nucleotide analogs based on aminonaphthalimides, **AN1-AN5**, and based on cyanovinylenes, **CV1** and **CV2**. Sequences of single-stranded (ss) and double-stranded **DNA1-DNA4X** with Illustration of the orientation in double helices. Green color is used for single dyes and orange for those DNA architectures with potential dye dimerization.

Bouffard et al. and Kim et al. reported cyanovinylenes forming fluorescent dimers with red-shifted emission in antiparallel orientations [23]. Both dyes offer several advantages as fluorescent DNA probes: (i) excitation beyond the cell-damaging UV-B range and (ii) an intrinsic ability to intercalate into DNA based on their flat molecule geometry. Herein, we present novel DNA building blocks that allow synthetic incorporation of aminonaphthalimides (**AN1-AN5**) and cyanovinylenes (**CV1-CV2**) fluorescent nucleotide surrogates into oligonucleotides (Figure 1). These building blocks were designed to explore the potential of both dyes for fluorescence readout by turn-on and red-shift in double-stranded DNA. Furthermore, we investigated (i) the influence of linker lengths representatively for the fluorescent properties of aminonaphthalimide in DNA, and (ii) the role of the alkylamino group for fluorescence response of the cyanovinylene in DNA. The chromophores were incorporated as single fluorophores into **DNA1** to evaluate their fluorescent properties, and as dimers, either in an interstrand orientation after annealing of two singly modified oligonucleotides (**DNA2**), or in an intrastrand orientation by oligonucleotides with two chromophore modifications (**DNA3** and **DNA4X**). The latter case is important for bioanalytical applications, in particular sequence-specific DNA and RNA probing. We evaluate these probes for the detection of N^6-methyl-2'-deoxyadenosine (m^6A) in DNA.

2 | Results and Discussion

2.1 | Synthesis of Building Blocks AN1-AN5 for DNA Modified With Aminonaphthalimide

Aminonaphthalimide was incorporated into oligonucleotides using (*S*)-2-amino-1,3-propandiol (**2b**, DMT-protected **5**) as an acyclic linker between the phosphodiester bridges. This chiral propanediol was chosen as linker because of its high stability and flexibility in comparison to conventional 2-deoxyfuranoside. It places the chromophore as nucleotide substitution into DNA and is compatible with automated oligonucleotide chemistry using phosphoramidites as building blocks [24]. Synthesis of DNA modifications **AN1-AN4** starts with 4-bromo-1,8-naphthalic acid anhydride that is converted into 4-*N*,*N*-dimethylamino-1,8-naphthalic acid anhydride **1a** and into 4-amino-1,8-naphthalic acid anhydride **1b** by nucleophilic substitution of the bromide by azide function and subsequent reduction of the azide group into the amino group by NaHS (see Supporting Information) [25–27]. For the first set of DNA building blocks **10a** and **10b** (Scheme 1), compounds **1a** and **1b** were directly condensed with (*S*)-2-amino-1,3-propanediol (**2b**) anchoring this linker at the imide nitrogen of **4a** and **4b** [24]. For later DNA synthesis, the amino function of **4b** had to be protected by dmf to **7b**. Both compounds **4a** and **7b** were converted into their phosphoramidites as building blocks for automated DNA synthesis by standard protocols including DMT protection at the primary hydroxy function to **8a** and **8b** and phosphitylation at the secondary hydroxy function to **10a** and **10b**. For the second set of DNA building blocks **9a** and **9b**, anhydrides **1a** and **1b** were first condensed with 3-aminopropane-1-ol (**2a**) to conjugates **3a** and **3b** anchoring this linker extension at the imide nitrogen of the chromophore. Here again, the amino function of **3b** had to be

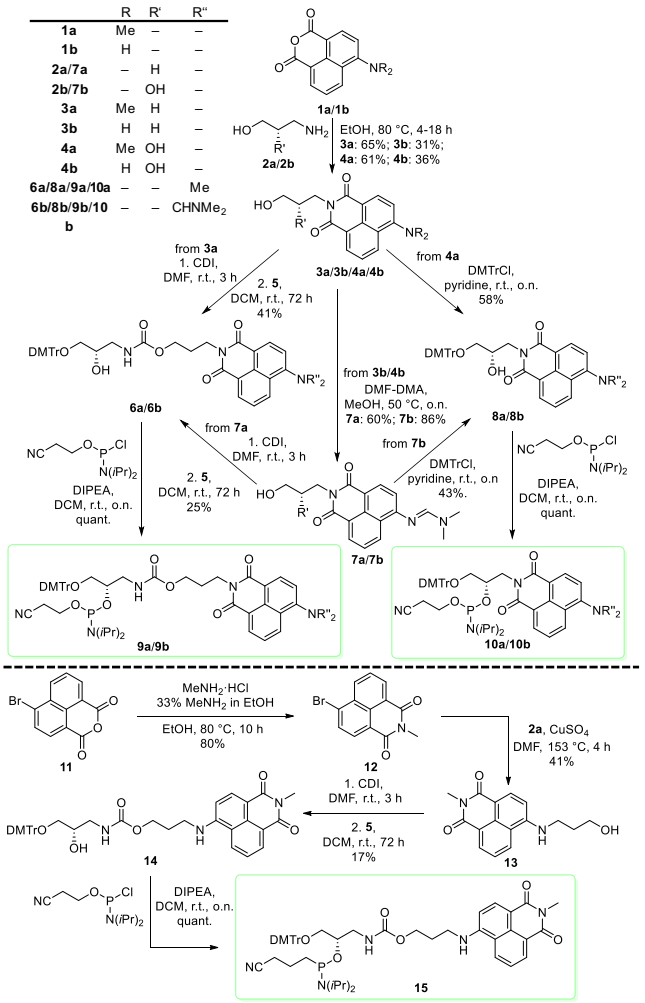

SCHEME 1 | Synthesis of phosphoramidites **9a**/**9b**, **10a**/**10b**, and **15** as building blocks for modification of DNA with nucleotide analogs **AN1**-**AN5**. For the structure of **5**, see Scheme 2.

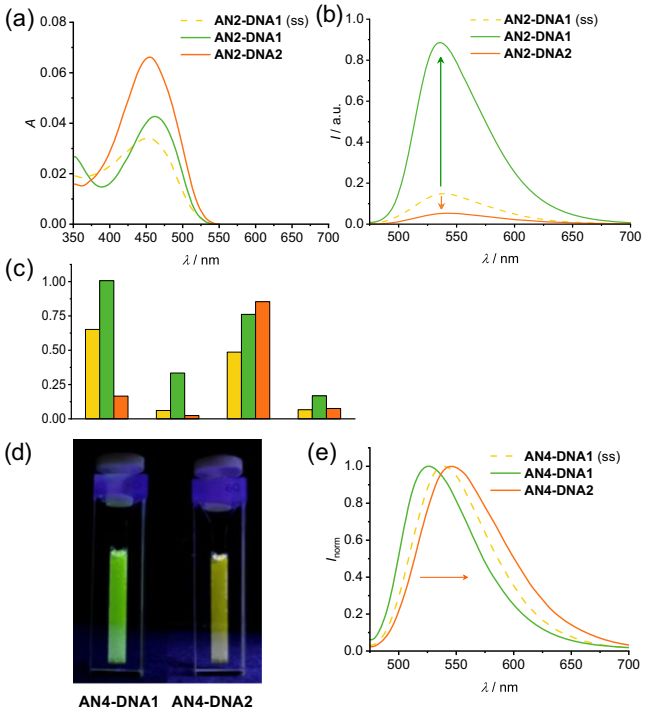

FIGURE 2 | (a) UV/Vis absorption and (b) fluoresence of single-stranded (ss) **AN2-DNA1**, **AN2-DNA1** and **AN2-DNA2** ($\lambda_{exc} = 460$ nm, 2.5 μM in 10 mM Na-P_i buffer, 250 mM NaCl, pH 7); (c) comparison of the fluorescence intensities of single-stranded (ss) **DNA1**, **DNA1** and **DNA2** modified with **AN1**, **AN2**, **AN3**, and **AN4** (left to right; $\lambda_{exc} = 460$ nm, 2.5 μM in 10 mM Na-P_i buffer, 250 mM NaCl, pH 7); (d) images of cuvettes filled with **AN4-DNA1** (left) and **AN4-DNA2** (right) ($\lambda_{exc} = 254$ nm with a handheld UV lamp, 2.5 μM in 10 mM Na-P_i buffer, 250 mM NaCl, pH 7); (e) normalized fluorescence of single-stranded (ss) **AN4-DNA1**, **AN4-DNA1**, **AN4-DNA2** ($\lambda_{exc} = 460$ nm, 2.5 μM in 10 mM Na-P_i buffer, 250 mM NaCl, pH 7).

protected by the dmf group to **7a** for later DNA synthesis. Both compounds **3a** and **7a** were then coupled with DMT-protected (*S*)-2-amino-1,3-propanediol **5** using 1,1-carbonyldimidiazol forming a urethane bridge. Both conjugates **6a** and **6b** were converted into their phosphoramidites **9a** and **9b** as building blocks for automated DNA synthesis. Compared to **AN1**-**AN4**, the DNA building block **AN5** bears aminonaphthalimide in the "inverted" orientation with the linker conjugated to the amino group instead of the imide group of the chromophore. The anhydride **11** was first converted into methylimide **12**, coupled with 3-aminopropanediol to **2a** yielding conjugate **13**, and then coupled to DMT-protected (*S*)-2-amino-1,3-propanediol **5** to nucleoside analog **14**. This was finally converted into phosphoramidite **15** as building block for automated synthesis of DNA modified with **AN5**.

2.2 | Optic-Spectroscopic Properties of Monomers and Interstrand Dimers of AN1-AN4 in DNA

The obtained phosphoramidites **9a**, **9b**, **10a**, and **10b** were incorporated into desired DNA sequences using automated oligonucleotide synthesis on 1 μmol scale on solid phase (CPG: controlled pore glass). Single-stranded (ss) **DNA1** and **DNA2** were modified with one chromophore, but they differ in their sequence to make them complementary to each other. In addition, the completely unmodified oligonucleotide was purchased, which is complementary to **DNA1**, and annealed to double-stranded **DNA1**. Single-stranded (ss) **DNA1** and **DNA2** were annealed to double-stranded **DNA2** forming an interstrand pair of the chromophores. In general, UV/Vis absorption and the fluorescence of aminonaphthalimide-modified DNA show a broad band without fine structure, typical for such push-pull-chromophore. Optic-spectroscopic properties are representatively discussed here for **AN2-DNA1**. The maximum of the UV/Vis absorption of single-stranded (ss) **AN2-DNA1** has its maximum at $\lambda = 454$ nm which shifts to $\lambda = 461$ nm after annealing of this strand with the complementary unmodified counterstrand to **AN2-DNA1** (Figure 2a). Thereby, the absorption at $\lambda = 454$ nm in the single strand indicates dye aggregation which is likely the result of an interaction between single dyes in two strands facilitated by folding of the single strand. This interaction is enforced by annealing to **AN2-DNA2** where two dyes are located close to each other forming an interstrand chromophore pair, and accordingly UV/Vis absorption occurs at $\lambda = 455$ nm. This dye dimer can also be observed by the fluorescence (Figure 2b).

When excited at $\lambda_{exc} = 460$ nm, fluorescence of **AN2-DNA2** occurs with a maximum at $\lambda = 540$ nm and a quantum yield of $\Phi_F = 1.3\%$. When the modified single strand is annealed with the complementary unmodified counterstrand to **AN2-DNA1**, fluorescence intensity strongly increases to $\Phi_F = 7.6\%$ and the maximum only slightly shifts to $\lambda = 536$ nm. The interstrand chromophore pair in **AN2-DNA2** shows a reduced fluorescence intensity of $\Phi_F = 0.08\%$ at $\lambda = 541$ nm. These dye properties are observed throughout the series of DNA modified with **AN1-AN4** chromophores (Figure 2c and Table 1). Although UV/Vis absorption and fluorescence of the **AN1**- and **AN3**-modified DNA occur at similar maxima as the **AN2**- and **AN4**-modified DNA, fluorescence intensities of the **AN1**- and **AN3**-modified DNA (bearing the non-methylated aminonaphthalimides) are generally higher compared to the **AN2**- and **AN4**-modified DNA (bearing methylated aminonaphthalimides) with quantum yields in the range $\Phi_F = 3.8–28.0\%$, and $\Phi_F = 17.3–25.8\%$, respectively. Fluorescence lifetimes extracted from decay maxima further support the described photophysical difference (Table 1). **AN1**- and **AN3**-modified DNA show longer average lifetimes in the range $\tau_0 = 3.42–11.85$ ns than **AN2**- and **AN4**-modified DNA with the range of $\tau_0 = 0.73–2.99$ ns, respectively, reflecting the previously observed monomeric emission. This difference can be explained by twisted intramolecular charge transfer (TICT), a well-known phenomenon occurring with dialkylated amino substituents [28]. Alternatively, the non-alkylated amino group of **AN4** might interact with the counterstrand by unspecific hydrogen bonding. With respect to a fluorescence shift as potential readout, the long linker in **AN4-DNA2** gave an interesting result (Figure 2d,e): the fluorescence maximum bathochromically shifts to $\lambda = 549$ nm with nearly unchanged fluorescence intensity of $\Phi_F = 1.8\%$ compared to the single-strand. According to our published result with TO as fluorescent nucleotide, these optical properties are typical for an excimer formation between two dyes and are a promising fluorescent readout [20].

TABLE 1 | UV/Vis absorption maxima λ_{abs}, fluorescence maxima λ_{em}, fluorescent quantum yields Φ_F, average fluorescence lifetime $\tau_ø$, and melting temperatures T_m of **AN1-**, **AN2-**, **AN3-**, and **AN4-DNA**, both single (ss) and double strands.

	λ_{abs}/ nm	λ_{em}/ nm	Φ_F	$\tau_Ø$/ ns	T_m/ °C
AN1-DNA1 (ss)	441	533	0.197	8.83	—
AN1-DNA1	454	534	0.280	10.12	60.0
AN1-DNA2	446	537	0.038	3.42	61.0
AN2-DNA1 (ss)	454	540	0.013	1.56	—
AN2-DNA1	461	536	0.076	2.99	60.0
AN2-DNA2	455	541	0.008	1.09	59.0
AN3-DNA1 (ss)	439	529	0.173	8.72	—
AN3-DNA1	441	526	0.258	11.85	65.3
AN3-DNA2	439	528	0.179	9.20	65.2
AN4-DNA1 (ss)	453	540	0.024	1.15	—
AN4-DNA1	455	527	0.045	1.54	64.5
AN4-DNA2	451	549	0.018	0.73	64.7

2.3 | Synthesis of Building Blocks CV1 and CV2 for DNA Modified with Cyanovinylene

Following the results gained with **AN1**- to **AN4**-modified DNA, especially the observed TICT behavior, the two CV building blocks differ in terms of aliphatic residues on the tertiary nitrogen. While nucleotide **CV1** contains ethyl moieties, presumably showing also TICT behavior in the excited state, nucleotide **CV2** features the anchored and thereby cyclized amino group restricting conformational flexibility and therefore prohibiting TICT states [28]. Both building blocks **CV1** and **CV2** bear the long linker, similar to **AN3** and **AN4**. To synthesize phosphoramidites **23a** and **23b** (Scheme 2), 3-bromopropanol (**18**) as linker extension was firstly added to the hydroxy group of the starting molecules (**16** and **17**) by nucleophilic substitution under basic conditions and bromide elimination. The prepared **19a** and **19b** were condensed with commercially available benzothiazoleacetonitrile (**20**). The resulting fluorophores **21a** and **21b** were equipped with the acyclic DMT-protected *S*-3-amino-1,2-propanediol **5** via a carbamate linker to **22a** and **22b** [24]. Finally, **22a** and **22b** were converted by 2-cyanoethyl *N*,*N*-diisopropylchlorophosphor-amidite into phosphoramidites **23a** and **23b**.

2.4 | Optic-Spectroscopic Properties of Monomers and Interstrand Dimers of CV1 and CV2 in DNA

The obtained phosphoramidites were incorporated into desired sequences using a slightly modified automated solid-phase DNA synthesis protocol applying ultramild conditions (see Supporting Information). All oligonucleotides exhibit absorption bands at $\lambda = 465$ nm and $\lambda = 500$ nm; however, they differ in their fine structure. Single-stranded (ss) **CV1-DNA1** has its absorption maximum at $\lambda = 465$ nm with a shoulder at $\lambda = 500$ nm (Figure 3a). The hypsochromic shoulder is more pronounced, indicating a dimer between both dyes which is likely the result of an interstrand interaction between single dyes in two strands facilitated by folding of the single strand. This was evidenced by concentration dependent UV/Vis absorption spectroscopy (Figure S120). In double-stranded **CV1-DNA1**, the maximum

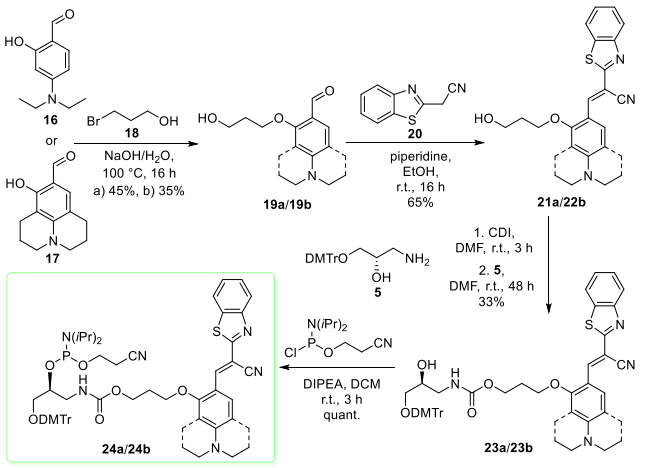

SCHEME 2 | Synthesis of phosphoramidites **23a** and **23b** as building blocks for modification of DNA with nucleotide analogs **CV1** and **CV2**.

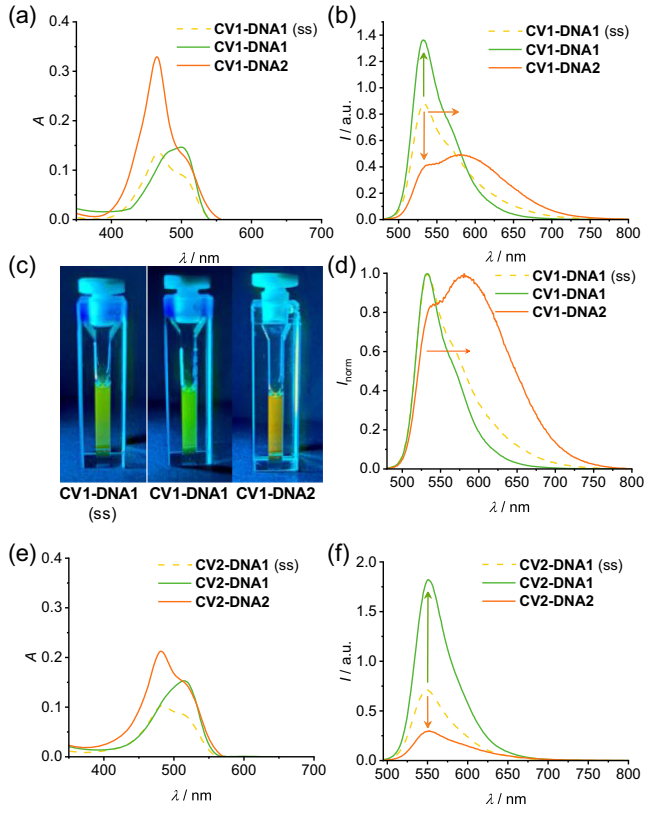

FIGURE 3 | (a) UV/Vis absorption and (b) fluorescence of single-stranded (ss) **CV1-DNA1**, **CV1-DNA1**, and **CV1-DNA2** ($\lambda_{exc} = 465$ nm, 2.5 μM in 10 mM Na-P_i buffer, 250 mM NaCl, pH 7); (c) images of cuvettes filled with single-stranded (ss) **CV1-DNA1**, **CV1-DNA1**, and **CV1-DNA2**, $\lambda_{exc} = 254$ nm with handheld UV lamp (2.5 μM in 10 mM Na-P_i buffer, 250 mM NaCl, pH 7); (d) normalized fluorescence of single-stranded (ss) **CV1-DNA1**, **CV1-DNA1**, and **CV1-DNA2** (2.5 μM in 10 mM Na-P_i buffer, 250 mM NaCl, pH 7); (e) UV/Vis absorption and (f) fluorescence of single-stranded (ss) **CV2-DNA1**, **CV2-DNA1**, and **CV2-DNA2** ($\lambda_{exc} = 480$ nm, 2.5 μM in 10 mM Na-P_i buffer, 250 mM NaCl, pH 7).

intensities are reversed and show the spectral features of the **CV1** monomer. The two dyes in **CV1-DNA2** are forced into close proximity, the hypsochromic dimer band at $\lambda = 465$ nm is significantly higher than the monomer band at $\lambda = 500$ nm; the latter is now a shoulder. These changes are characteristic for a chromophore dimer and observed in **CV1-DNA2** [20]. The absorption bands of **CV2** in DNA behave similarly but do not show such significant changes (Figure 3e). **CV2-DNA1** (ss), **CV2-DNA1**, and **CV2-DNA2** show absorption bands at $\lambda = 482$ nm and $\lambda = 515$ nm. As for **CV1**, the hypochromic shoulder at $\lambda = 482$ nm is more pronounced for **CV2-DNA1** (ss) and **CV2-DNA2**. For **CV2-DNA1**, the shoulder at 515 nm is more pronounced. However, the differences of the relative absorption band intensities are less pronounced, indicating a weaker dye-dye interaction compared to **CV1**. Fluorescence was measured by excitation at $\lambda = 465$ nm for **CV1**, and at $\lambda = 480$ nm for **CV2**. **CV1-DNA1** (ss), **CV1-DNA1**, and **CV1-DNA2** show their fluorescence with a maximum at $\lambda = 532$ nm (Figure 3b). Remarkably, **CV1-DNA1** (ss) and **CV1-DNA2** have a second emission at $\lambda = 570$ or $\lambda = 582$ nm, respectively. In **CV1-DNA2,** the bathochromically shifted shoulder is even the fluorescence maximum, and in addition, the fine structure is lost and a broad, structureless fluorescence occurs. In contrast, **CV1-DNA1** shows a fluorescence at $\lambda = 532$ nm with some fine structure indicating the optical properties of the **CV1** monomer. Single-stranded (ss) **CV1-DNA1** exhibits a quantum yield of $\Phi_F = 6.6\%$, which rises slightly to $\Phi_F = 7.1\%$ upon hybridization to double-strand **CV1-DNA1**. With respect to the concentration-dependent UV/Vis absorption indicating interstrand dye-dye interactions as discussed above, the use of single-strand fluorescence might be problematic in applications. In contrast, the bathochromically shifted fluorescence of **CV1-DNA2** shows a partially quenched quantum yield of $\Phi_F = 4.5\%$. Taken together, these optical properties are characteristic for an excimer in DNA formed by the interstrand pair of dye **CV1** yielding a characteristic change of fluorescence color readout from green to orange [20]. **CV2-DNA1** (ss), **CV2-DNA1**, and **CV2-DNA-2** show their fluorescence maximum at $\lambda = 550$ nm (Figure 3f). Here, fluorescence without shoulders is obtained suggesting pure monomeric emission of **CV2**. The differences in quantum yields are, however, remarkably different. The quantum yield of the single-stranded (ss) **CV2-DNA1** rises from $\Phi_F = 13.1\%$ to $\Phi_F = 31.4\%$ upon hybridization to double strand **CV2-DNA1**. In **CV2-DNA2**, fluorescence is quenched to $\Phi_F = 3.9\%$ probably by dye-dye interaction. **CV2** thus acts as a hybridization-sensitive dye, reporting duplex formation through a significant fluorescence turn-on. The distinct optic-spectroscopic behavior of the two building blocks **CV1** and **CV2** can be attributed to differences in rotational freedom of their substituents. **CV1** contains rotatable ethyl groups, which -in the three-dimensional structure of double-helical DNA- allows formation of a fluorescent dimer. In contrast, the rigidly cyclized substituents of **CV2** prevent such dimer formation, as the chromophores lack conformational flexibility required to adopt the proper angle and orientation for this interaction. For both, **CV1** and **CV2**, fluorescence increases upon hybridization from single-stranded **DNA1** to double stranded **DNA1**. This turn-up effect is significantly more pronounced for **CV2**. This enhanced response can likewise be ascribed to the reduced conformational mobility of its chromophore.

Fluorescence lifetimes extracted from the decay maxima further corroborate the distinct photophysical behavior (Table 2). Single-stranded (ss) **CV1-DNA1**, **CV1-DNA1**, and **CV1-DNA2** show average lifetimes of $\tau_0 = 0.83$ ns, $\tau_0 = 0.55$ ns and $\tau_0 = 1.18$ ns, respectively, reflecting the previously observed monomeric emission of **CV1-DNA1** and the elongated lifetime for the excimer emission of **CV1-DNA2**. In contrast, single-stranded (ss) **CV2-DNA-1**, **CV2-DNA-1**, and **CV2-DNA-2** exhibit comparable average lifetimes within a narrow range of $\tau_0 = 1.28$ – $\tau_0 = 1.48$ ns, indicating the absence of detectable excimer emission of **CV2** in DNA. In general, conformational flexibility of chromophores facilitates nonradiative decay pathways and thus quenches fluorescence. Hybridization restricts rotational freedom in the vinyl bridge of both dyes, yet in **CV1** the ethyl substituents remain rotatable and may induce quenching through formation of a TICT state. Such a pathway is not accessible in **CV2**, rendering this dye more sensitive to hybridization. Notably, the bathochromic shift of emissions of **CV1** in DNA can be seen with the naked eye using a handheld UV lamp for excitation at $\lambda = 254$ nm (Figure 3c,d). **CV1-DNA-1** (ss) exhibits a yellowish-green fluorescence. The yellow tint in the emission is due to the slight dimer shoulder at $\lambda = 582$ nm. **CV1-DNA-1** fluoresces by a green color because of the monomer emission at $\lambda = 532$ nm. **CV1-DNA-2**

TABLE 2 | UV/Vis absorption maxima λ_{abs}, fluorescence maxima λ_{em}, fluorescent quantum yields Φ_F, average fluorescence lifetime $\tau_ø$, and melting temperatures T_m of **CV1**- and **CV2**-modified single and double strands **DNA1** and **DNA2**.

	λ_{abs}/nm	λ_{em}/nm	Φ_F	$\tau_Ø$/ns	T_m/°C
CV1-DNA1 (ss)	465/500	532/570	0.066	0.83	—
CV1-DNA1	500	532	0.071	0.55	60.0
CV1-DNA2	465	582	0.045	1.18	65.5
CV2-DNA1 (ss)	482/515	550	0.131	1.48	—
CV2-DNA1	515	550	0.314	1.28	60.5
CV2-DNA2	482/515	550	0.039	1.31	67.5

fluoresces by an orange color because of the bathochromically shifted excimer emission at $\lambda = 582$ nm.

2.5 | Intrastrand Dimers of CV1 and AN3 in DNA and Fluorescent Probing of 6-Methyladenosine (m^6A)

The chromophore building blocks **CV1** and **AN4** were incorporated twice adjacent to each other into the same strand in **DNA3** to investigate their potential intrastrand interactions. Both dyes were selected because they showed substantial amounts of dimers in the interstrand orientation in **CV1-DNA2** and **AN4-DNA2**, as described in the previous paragraphs (see Figures 2d,e and 3c,d). In contrast to the interstrand dimer of **DNA2**, the dyes are arranged in a parallel rather antiparallel orientation (Figure 4a). Single-stranded (ss) **CV1**- and **AN4-DNA3** were annealed with the complementary oligonucleotide to corresponding double strands **CV1**- and **AN4-DNA3**. Cytidines were placed opposite to the chromophores into the counterstrands. Dimer formation can be clearly seen for **CV1-DNA3**. For this double strand, an absorption maximum at $\lambda = 466$ nm with a shoulder at $\lambda = 500$ nm is observed (Figure S112). Since the hypsochromically shifted shoulder is more pronounced, the absorption suggest dye-dye interactions in **CV1-DNA3**. Single-strand **CV1-DNA3** (ss) shows also this spectroscopic signature. Obviously, hybridization does not noticeably affect the absorption. Their fluorescence was recorded by excitation at 465 nm (Figure 4b and Table 3). When **CV1** is incorporated twice, as in **CV1-DNA3** (ss) and **CV1-DNA3**, the emission maximum occurs at $\lambda = 535$ nm with a shoulder at $\lambda = 575$ nm that is nearly equally intense. This indicates that both single and double strand exhibit not only monomeric emission but also a substantial contribution from excimer emission. In case of **CV1-DNA4** (ss) one T has been placed between the two dyes. Upon hybridization to **CV1-DNA4A**, the ratio of monomer to excimer emission decreases, accompanied by an increase in quantum yield. The intervening T-A pair, a matched Watson-Crick base pair, between the dyes in **CV1-DNA4A** completely blocks the interaction of this dye pair, whereas the T–T mismatch in **CV1-DNA4T** allows the dimerization to a certain extent, probably by bulging out the Ts of the duplex (Figure 4a). There are two indications for dimerization in **CV1-DNA4T**. (i) Fluorescence is quenched; the quantum yield drops from $\Phi_F = 3.5\%$ for **CV1-DNA4A** to $\Phi_F = 3.0\%$ for **CV1-DNA4T**. (ii) A broad shoulder between $\lambda = 536$ nm and $\lambda = 573$ nm occurs in the fluorescence of **CV1-DNA4T**. According to the bathochromically shifted fluorescence of **CV1-DNA2** at $\lambda = 582$ nm, this shows excimer formation of **CV1** also as an intrastrand pair. These fluorescence changes potentially allow to probe m^6A. m^6A is the most prevalent and natural DNA modification in prokaryotes to distinguish own DNA from potential dangerous other DNA [29, 30]. m^6A is also important for DNA repair and regulation in Escherichia coli and other bacteria. Although m^6A is under debate in mammals, m^6A was recently found as genome-wide modification of DNA of eukaryotes, including plants and mammals, and associated with a variety of potential biological roles [31–34]. Understanding the biological function of m^6A requires detection and mapping of this DNA modification. The conformational equilibrium in the T-m^6A pair, in particular syn- and anticonformation of m^6A, is an interesting property that places the T-m^6A pair structurally between a

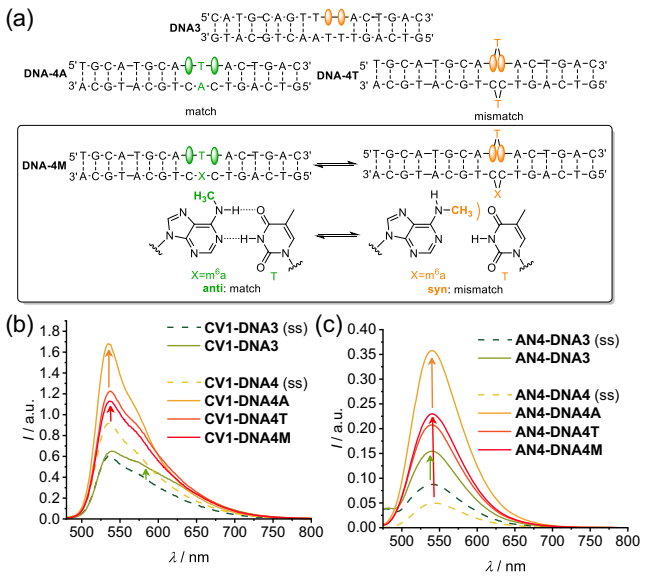

FIGURE 4 | (a) Sequences of **DNA3** and **DNA4-A/T/M**, modified with either two **CV1** or two **AN4** nucleotide analogs directly adjacent to each other or separated by one A. Green color is used for clearly separated dyes and orange for those DNA architectures with potential dye dimerization. The correct A-T pair in **DNA4-A** separates both dyes, whereas the T–T mismatch in **DNA4-T** allows dye dimerization. **DNA4-M** shows an equilibrium between fully matched and mismatched double strand by the anti-syn isomerization of m^6A. (b) fluorescence of single-stranded (ss) **CV1-DNA3**, **CV1-DNA3**, single-stranded (ss) **CV1-DNA4** and **CV1-DNA4A/T/M**, $\lambda_{exc} = 465$ nm (2.5 μM in 10 mM Na-P_i buffer, 250 mM NaCl, pH7); and fluorescence of single-stranded (ss) **AN4-DNA3**, **AN4-DNA3**, single-stranded (ss) **AN4-DNA4** and **AN4-DNA4A/T/M**, $\lambda_{exc} = 465$ nm (2.5 μM in 10 mM Na-P_i buffer, 250 mM NaCl, pH7.

TABLE 3 | UV/Vis absorption maxima λ_{abs}, fluorescence maxima λ_{em}, fluorescent quantum yields Φ_F, average fluorescence lifetime $\tau_ø$, and melting temperatures T_m of **CV1**- and **AN4**-modified single and double strands **DNA3** and **DNA4**.

	λ_{abs}/nm	λ_{em}/nm	Φ_F	$\tau_Ø$/ns	T_m/°C
CV1-DNA3 (ss)	466/500	535/575	0.026	0.45	—
CV1-DNA3	466/500	535/575	0.029	0.30	49.5
CV1-DNA4 (ss)	470/500	536	0.029	0.47	—
CV1-DNA4A	470/500	536	0.035	0.46	49.0
CV1-DNA4T	470/500	536	0.030	0.42	46.5
CV1-DNA4M	470/500	536	0.030	0.43	48.5
AN4-DNA3 (ss)	448	542	0.013	1.29	—
AN4-DNA3	454	540	0.015	1.55	57.2
AN4-DNA4 (ss)	453	541	0.004	0.52	—
AN4-DNA4A	451	540	0.026	0.92	58.8
AN4-DNA4T	448	540	0.017	0.44	56.3
AN4-DNA4M	451	540	0.018	0.75	57.5
AN4-AN5-DNA3 (ss)	451	541	0.046	3.30	—
AN4-AN5-DNA3	452	538	0.045	3.11	56.8
AN4-AN5-DNA4 (ss)	453	538	0.027	2.79	—
AN4-AN5-DNA4A	455	538	0.071	3.24	56.3
AN4-AN5-DNA4T	452	536	0.064	3.05	53.0
AN4-AN5-DNA4M	453	538	0.064	3.02	55.3

full match (T-A) and a mismatch (T-T). In the anticonformation, hydrogen bonding to T is not perturbed leading to a base pair match and interrupting the interaction of the chromophores. In contrast, the hydrogen bonding to T is hindered by the methyl group in the syn-conformation and the pairing is similar to a mismatch. In fact, the fluorescence of **CV1-DNA4M** is a mixture of both, **CV1** monomer and excimer fluorescence, as indicated by fluorescence intensity and shoulder around 573 nm. In comparison, the UV/Vis absorption of **AN4-DNA3** modified with two chromophores **AN4**, the missing fine structure does not allow to follow dimer formation in these duplexes by their absorbance as discussed above for **CV1-DNA3**. However, the fluorescence intensity of **AN4-DNA4A** ($\Phi_F = 2.6\%$) with intact T-A pair between the two dyes in comparison to the lower intensity of **AN4-DNA4T** ($\Phi_F = 1.7\%$) with T-T mismatch evidences also intrastrand dimerization of the two dyes **AN4** (Figure 4c and Table 3). Here again, the pair between T and m^6A in **AN4-DNA4M** behaves both as a match (due to the anticonformation of m^6A) and a mismatch (due to the syn-conformation of m^6A). Accordingly, the fluorescence shows more intensity typical for the mismatch ($\Phi_F = 1.8\%$). We synthesized also **AN4-AN5-DNA3** and **AN4-AN5-DNA4**, in which the chromophores **AN4** and **AN5** were placed either adjacent to each other or with an intervening T (Figures S119). This chromophore pair has an antiparallel orientation by the different attachment of the linker to the chromophores, and should thereby mimic the orientation of the interstrand pair of **AN4-DNA2**. For the two adjacent chromophores of **AN4-AN5-DNA3** the results were analogs to **AN4-DNA3** and the missing fine structure prevents any conclusion on dimer formation. Unexpectedly, **AN4-AN5-DNA4** showed neither a red-shifted excimer fluorescence (as **AN4-DNA2**) nor a significant fluorescence turn-on with the possibility to probe the T-m^6A pair between the two different dyes (as **AN4-DNA4**).

3 | Conclusion

In this work, we have introduced aminonaphthalimides and cyanovinylenes as novel fluorescent nucleotide analogs into DNA and systemically evaluated their photophysical behavior. The chromophores were attached to oligonucleotides using an acyclic linker between the phosphodiester bridges. The chiral propanediol as linker provides high stability and flexibility in comparison to the conventional 2-deoxyfuranoside; it places the chromophore as nucleotide substitution into DNA and is compatible with automated oligonucleotide chemistry using phosphoramidites as building blocks. For aminonaphthalimides **AN1**-**AN4**, we compared two different linker lengths and evaluated the role of demethylation at the exocyclic amino group. The shorter linker in **AN1-DNA2** and **AN2-DNA2** induces dye–dye interactions that efficiently quench their fluorescence. These interactions were even observed in the single-strand **AN1-DNA1** and **AN2-DNA1**. As a result, these DNA strands can be used light-up probes for complementary oligonucleotides, because the fluorescence intensity increases significantly to their double strands. The longer linker in **AN3-DNA2** and **AN4-DNA2** modulate interstrand dye–dye interactions such that not only a fluorescence quenching is observed by the dye interaction but an additional red-shift by the excimer fluorescence, most pronounced in **AN4-DNA2** for which the fluorescence color turns from green to yellow. The fluorescence intensities of the non-methylated chromophores **AN1** and **AN3** in DNA are generally higher than the methylated **AN2** and **AN4** in DNA. This difference can most likely be explained by twisted intramolecular charge transfer (TICT), a well-known phenomenon occurring with dialkylated amino substituents. For cyanovinylenes **CV1** and **CV2**, the role of the alkylamino group for the fluorescence response was evaluated. The attachment of the alkyl substituents to the

chromophore core in **CV2** prevents the formation of TICT states. Similar to aminophthalimide-modified DNA, significant fluorescence quenching was observed by interstrand dye interactions in **CV1-DNA1** and **CV2-DNA**. These interactions were even observed in single strands **CV1-DNA1** and **CV2-DNA1;** the fluorescence contrast was higher with **CV2**. Therefore, **CV2-DNA1** emerges as a hybridization reporter with an excitation in the visible light range ($\lambda = 480$ nm). On the other hand, in **CV1-DNA2**, a red-shifted excimer fluorescence was observed by interstrand dye interactions which turns the fluorescence color from green to orange. This fluorescence shift was more significant than the one observed for **AN4-DNA2**. In conclusion, elucidation of these optic-spectroscopic properties underscores the versatility of aminonaphthalimides and cyanovinylenes as nucleic acid-sensitive dyes and thereby expands the available toolbox of fluorescent probes for nucleic acids with turn-on and red-shift as readouts. These fluorescence changes allow to probe N^6-methyl-2′-deoxyadenosine (m^6A) based on the syn-/anticonformation mixtures of the N^6-methyl group rendering this naturally modified base pair a partial mismatch.

Acknowledgments

Financial support by the Deutsche Forschungsgemeinschaft (DFG, grant Wa 1386/26-1) and the Karlsruhe Institute of Technology is gratefully acknowledged.

Open Access funding enabled and organized by Projekt DEAL.

Funding

This work was supported by the Deutsche Forschungsgemeinschaft (Wa 1386/26−1).

Data Availability Statement

The data that supports the findings of this study are available in the supplementary material of this article.

References

1. V. V. Didenko, "DNA Probes Using Fluorescence Resonance Energy Transfer (FRET): Designs and Applications," *BioTechniques* 31 (2001): 1106–1121.

2. J. Gebhard, L. Hirsch, C. Schwechheimer, and H.-A. Wagenknecht, "Hybridization-Sensitive Fluorescent Probes for DNA and RNA by a Modular "Click" Approach," *Bioconjugate Chemistry* 33 (2022): 1634–1642.

3. C. Holzhauser, and H.-A. Wagenknecht, "DNA and RNA "Traffic Lights": Synthetic Wavelength-Shifting Fluorescent Probes Based on Nucleic Acid Base Substitutes for Molecular Imaging," *The Journal of Organic Chemistry* 78 (2013): 7373–7379.

4. J. G. Wetmur, "DNA Probes: Applications of the Principles of Nucleic Acid Hybridization," *Critical Reviews in Biochemistry and Molecular Biology* 26 (2008): 227–259.

5. J. Isacsson, H. Cao, L. Ohlsson, et al., "Rapid and Specific Detection of PCR Products Using Light-up Probes," *Molecular and Cellular Probes* 14 (2000): 321–328.

6. J. Hoche, H.-C. Schmitt, A. Humeniuk, I. Fischer, R. Mitrić, and M. I. S. Röhr, "The Mechanism of Excimer Formation: An Experimental and Theoretical Study on the Pyrene Dimer," *Physical Chemistry Chemical Physics* 19 (2017): 25002–25015.

7. C. Chen, B. Zhou, D. Lu, and G. Xu, "Electron Transfer Events in Solutions of Cyanine Dyes," *Journal of Photochemistry and Photobiology A: Chemistry* 89 (1995): 25–29.

8. A. Okamoto, T. Ichiba, and I. Saito, "Pyrene-Labeled Oligodeoxynucleotide Probe for Detecting Base Insertion by Excimer Fluorescence Emission," *Journal of the American Chemical Society* 126 (2004): 8364–8365.

9. M. Masuko, H. Ohtani, K. Ebata, and A. Shimadzu, "Optimization of Excimer-Forming Two-Probe Nucleic Acid Hybridization Method with Pyrene as a Fluorophore," *Nucleic Acids Research* 26 (1998): 5409–5416.

10. S. M. Langenegger, and R. Häner, "Excimer Formation by Interstrand Stacked Pyrenes," *Chemical Communications* 24 (2004): 2792–2793.

11. G. Tong, J. M. Lawlor, G. W. Tregear, and J. Haralambidis, "Oligonucleotide-Polyamide Hybrid Molecules Containing Multiple Pyrene Residues Exhibit Significant Excimer Fluorescence," *Journal of the American Chemical Society* 117 (1995): 12151–12158.

12. E. Mayer-Enthart and H. A. Wagenknecht, "Structure-Sensitive and Self-Assembled Helical Pyrene Array Based on DNA Architecture," *Angewandte Chemie International Edition* 45 (2006): 3372.

13. T. A. Zeidan, R. Carmieli, R. F. Kelley, T. M. Wilson, F. D. Lewis, and M. R. Wasielewski, "Charge-Transfer and Spin Dynamics in DNA Hairpin Conjugates With Perylenediimide as a Base-Pair Surrogate," *Journal of the American Chemical Society* 130 (2008): 13945–13955.

14. C. Wagner, and H.-A. Wagenknecht, "Perylene-3,4:9,10-tetracarboxylic Acid Bisimide Dye as an Artificial DNA Base Surrogate," *Organic Letters* 8 (2006): 4191–4194.

15. O. Seitz, F. Bergmann, and D. Heindl, "A Convergent Strategy for the Modification of Peptide Nucleic Acids: Novel Mismatch-Specific PNA-Hybridization Probes," *Angewandte Chemie International Edition* 38 (1999): 2203–2206.

16. F. Hövelmann, L. Bethge, and O. Seitz, "Single Labeled DNA FIT Probes for Avoiding False-Positive Signaling in the Detection of DNA/RNA in qPCR or Cell Media," *ChemBioChem* 13 (2012): 2072–2081.

17. L. Bethge, I. Singh, and O. Seitz, "Designed Thiazole Orange Nucleotides for the Synthesis of Single Labelled Oligonucleotides that Fluoresce Upon Matched Hybridization," *Organic & Biomolecular Chemistry* 8 (2010): 2439–2448.

18. S. Ikeda, T. Kubota, M. Yuki, H. Yanagisawa, S. Tsuruma, and A. Okamoto, "Hybridization-Sensitive Fluorescent DNA Probe With Self-Avoidance Ability," *Organic & Biomolecular Chemistry* 8 (2010): 546–551.

19. A. Okamoto, "ECHO Probes: A Concept of Fluorescence Control for Practical Nucleic Acid Sensing," *Chemical Society Reviews* 40 (2011): 5815–5828.

20. S. Berndl and H. A. Wagenknecht, "Fluorescent Color Readout of DNA Hybridization With Thiazole Orange as an Artificial DNA Base," *Angewandte Chemie International Edition* 48 (2009): 2418–2421.

21. S. Berndl, S. D. Dimitrov, F. Menacher, T. Fiebig, and H. A. Wagenknecht, "Thiazole Orange Dimers in DNA: Fluorescent Base Substitutions With Hybridization Readout," *Chemistry–A European Journal* 22 (2016): 2386–2395.

22. Z. Xu, J. Pan, D. R. Spring, J. Cui, and J. Yoon, "Ratiometric Fluorescent and Colorimetric Sensors for Cu2+ Based on 4, 5-Disubstituted-1, 8-Naphthalimide and Sensing Cyanide via Cu2+ Displacement Approach," *Tetrahedron* 66 (2010): 1678–1683.

23. G. Han, D. Kim, Y. Park, J. Bouffard, and Y. Kim, "Excimers Beyond Pyrene: A Far-Red Optical Proximity Reporter and Its Application to the Label-Free Detection of DNA," *Angewandte Chemie* 13 (2015): 3984–3988.

24. A. V. Azhayev and M. L. Antopolsky, "Amide Group Assisted 3′-Dephosphorylation of Oligonucleotides Synthesized on Universal A-Supports," *Tetrahedron* 57 (2001): 4977–4986.

25. R. Al-Aqar, A. Atahan, A. C. Benniston, T. Perks, P. G. Waddell, and A. Harriman, "Exciton Migration and Surface Trapping for a Photonic Crystal Displaying Charge-Recombination Fluorescence," *Chemistry–A European Journal* 22 (2016): 15420–15429.

26. M. D. Tomczyk, A. Byczek-Wyrostek, K. Strama, M. Wawszków, P. Kasprzycki, and K. Z. Walczak, "Anticancer Activity and Topoisomerase II Inhibition of Naphthalimides with ω-Hydroxylalkylamine Side-Chains of Different Lengths," *Medicinal Chemistry* 15 (2019): 550–560.

27. Z. R. Grabowski, K. Rotkiewic, and W. Rettig, "Structural Changes Accompanying Intramolecular Electron Transfer: Focus on Twisted Intramolecular Charge-Transfer States and Structures," *Chemical Reviews* 103 (2003): 3899–4032.

28. A. K. Satpati, M. Kumbhakar, S. Nath, and H. Pal, "Photophysical Properties of Coumarin-7 Dye: Role of Twisted Intramolecular Charge Transfer State in High Polarity Protic Solvents," *Photochemistry and Photobiology* 85 (2009): 119–129.

29. G. Z. Luo, M. A. Blanco, E. L. Greer, C. He, and Y. Shi, "DNA N. 6-Methyladenine: A New Epigenetic Mark in Eukaryotes?," *Nature Reviews Molecular Cell Biology* 16 (2015): 705–710.

30. Z. K. O'Brown and E. L. Greer, "N6-Methyladenine: A Conserved and Dynamic DNA Mark," *DNA Methyltransferases-Role and Function* (2016): 213–246.

31. C. Shen, K. Wang, X. Deng, and J. Chen, "DNA N6-Methyldeoxyadenosine in Mammals and Human Disease," *Trends in Genetics* 38 (2022): 454–467.

32. M. U. Musheev, A. Baumgärtner, L. Krebs, and C. Niehrs, "The Origin of Genomic N. 6-Methyl-Deoxyadenosine in Mammalian Cells," *Nature Chemical Biology* 16 (2020): 630–634.

33. L. Q. Chen, Z. Zhang, H. X. Chen, et al., "High-Precision Mapping Reveals Rare N. 6-Deoxyadenosine Methylation in the Mammalian Genome," *Cell Discovery* 8 (2022): 138.

34. Y. Fu, G. Z. Luo, K. Chen, et al., "N6-Methyldeoxyadenosine Marks Active Transcription Start Sites in Chlamydomonas," *Cell* 161 (2015): 879–892.

Supporting Information

Additional supporting information can be found online in the Supporting Information section.